APR 3 1997

SANDIA REPORT

SAND97-0507 • UC-213
Unlimited Release
Printed March 1997

Degradation of the Materials of Construction in Li-Ion Batteries

RECEIVED
APR 16 1997
OSTI

Jeffrey W. Braithwaite, Angelo Gonzales, Samuel J. Lucero, Diane E. Peebles, James A. Ohlhausen, Wendy R. Cieslak, Ganesan Nagasubramanian

Prepared by
Sandia National Laboratories
Albuquerque, New Mexico 87185 and Livermore, California 94550

Sandia is a multiprogram laboratory operated by Sandia Corporation, a Lockheed Martin Company, for the United States Department of Energy under Contract DE-AC04-94AL85000.

DISTRIBUTION OF THIS DOCUMENT IS UNLIMITED

Approved for public release; distribution is unlimited.

Sandia National Laboratories

MASTER

SF2900Q(8-81)

Issued by Sandia National Laboratories, operated for the United States Department of Energy by Sandia Corporation.
NOTICE: This report was prepared as an account of work sponsored by an agency of the United States Government. Neither the United States Government nor any agency thereof, nor any of their employees, nor any of their contractors, subcontractors, or their employees, makes any warranty, express or implied, or assumes any legal liability or responsibility for the accuracy, completeness, or usefulness of any information, apparatus, product, or process disclosed, or represents that its use would not infringe privately owned rights. Reference herein to any specific commercial product, process, or service by trade name, trademark, manufacturer, or otherwise, does not necessarily constitute or imply its endorsement, recommendation, or favoring by the United States Government, any agency thereof, or any of their contractors or subcontractors. The views and opinions expressed herein do not necessarily state or reflect those of the United States Government, any agency thereof, or any of their contractors.

Printed in the United States of America. This report has been reproduced directly from the best available copy.

Available to DOE and DOE contractors from
Office of Scientific and Technical Information
P.O. Box 62
Oak Ridge, TN 37831

Prices available from (615) 576-8401, FTS 626-8401

Available to the public from
National Technical Information Service
U.S. Department of Commerce
5285 Port Royal Rd
Springfield, VA 22161

NTIS price codes
Printed copy: A03
Microfiche copy: A01

SAND97-0507
Unlimited Release
Printed March 1997

Distribution
Category UC-213

Degradation of the Materials of Construction in Li-Ion Batteries

Jeffrey W. Braithwaite, Angelo Gonzales,
Samuel J. Lucero, Diane E. Peebles,
James A. Ohlhausen, and Wendy R. Cieslak
Materials Aging and Reliability: Interfaces Department

Ganesan Nagasubramanian
Lithium Battery Research and Development Department

Sandia National Laboratories
PO Box 5800
Albuquerque, NM 87185-0340

Abstract

The primary current-collector materials being used in lithium-ion cells are susceptible to environmental degradation: aluminum to pitting corrosion and copper to environmentally assisted cracking. Pitting occurs at the highly oxidizing potentials associated with the positive-electrode charge condition. However, the pitting mechanism is more complex than that typically observed in aqueous systems in that the pits are filled with a mixed metal/oxide product and exist as mounds or nodules on the surface. Electrochemical impedance spectroscopy was shown to be an effective analytical tool for quantifying and verifying aluminum corrosion behavior. Two fluorocarbon-based coatings were shown to improve the resistance of Al to pitting attack. Detailed x-ray photoelectron spectroscopy (XPS) surface analyses showed that there was very little difference in the films observed after simple immersion in either PC:DEC or EC:DMC electrolytes versus those following electrical cycling. Li and P are the predominant surface species. Finally, environmental cracking of copper can occur at or near the lithium potential and only if specific metallurgical conditions exist (work-hardening and large grain size).

INTRODUCTION

Advanced rechargeable lithium-ion batteries are presently being developed and commercialized worldwide for use in consumer electronic and electric vehicle applications. The motivation behind these efforts involves a favorable combination of energy and power density, service life, cost, and safety. High interest also exists for the specialized low-volume applications (e.g., military and aerospace) where higher reliability and possibly longer service life will be required. Long-term chemical degradation of the cell hardware materials can adversely affect electrical performance, life, and/or safety through (1) increased electrical resistance or even loss of continuity, (2) production of corrosion products that attack or passivate the active materials, (3) introduction of contaminants that also react with active materials (due to loss of cell hermeticity), and (4) loss of electrolyte. Typically, consumer battery technologies are re-engineered after these secondary types of materials problems become identified.

Potentially serious corrosion problems have been observed in primary lithium batteries. For example, environmentally assisted cracking (EAC) can occur at highly stressed portions of the nickel anode current collector grid in $Li/SOCl_2$ cells, an effect related to alkali-metal embrittlement [1,2]. An example of a cracked grid section is shown in Figure 1. In Li/SO_2 cells, EAC of the nickel-plated carbon steel container has reduced service life [3]. Additionally, unacceptable chemical degradation of the glass/metal seal occurred in both of these primary cell technologies [2].

Similar corrosion mechanisms may ultimately be encountered in the emerging rechargeable lithium-ion battery technology. This, along with the observation that many developers have noticed a significant resistance rise in some rechargeable Li-cell configurations, motivated a dedicated study to determine if reliability and service life will be compromised by chemical degradation of the materials of construction. The portion of this study that is described in this paper involved an identification of the major materials degradation issues, with the focus on corrosion of the aluminum positive current collector and EAC of the copper negative current collector. Degradation of polymeric materials has not yet been considered.

EXPERIMENTAL

Corrosion Behavior

The corrosion characteristics of aluminum alloys 1100 (99.0% min and 0.12% Cu) and 1145 (99.45% min) and copper alloy 110 (99.9% min) were studied in flooded half-cells that had a standard 3-electrode configuration (Figure 2). These cells contained a relatively large excess of electrolyte compared to actual cells to help ensure constant conditions over the extended period of the experiments. The cell container was a 10-ml Nalgene bottle with three metal feed-through seals placed in the lid that also functioned as points of attachment for the electrodes. The cell containers were vacuum leak checked prior to assembly to ensure hermeticity (maximum leak rate of 4×10^{-5} cc/sec). A platinum counter and the aluminum or copper working electrode were each spot-welded to a small strip of nickel, which was then subsequently spot welded to the tip of

DISCLAIMER

Portions of this document may be illegible in electronic image products. Images are produced from the best available original document.

one of the feed-throughs. Similarly, a lithium reference electrode was cold welded to a strip of nickel that was also spot welded to a feed-through. The platinum and working electrodes were approximately 1 cm x 1 cm (1 cm^2 area) and were positioned facing each other with a separation of approximately 0.5 cm. The lithium electrode was positioned perpendicular to and along side the other two electrodes, close to their edges. The 100-μm thick working electrodes were coated with polyvinylidene fluoride (PVDF) following spot-welding but prior to cell assembly on the side facing away from the counter electrode.

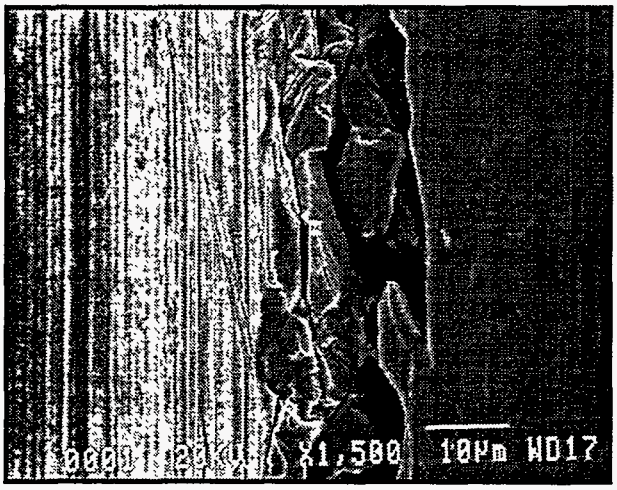

Figure 1. SEM photograph of the brittle fracture observed in a Ni test coupon aged in a $Li/SOCl_2$ cell environment.

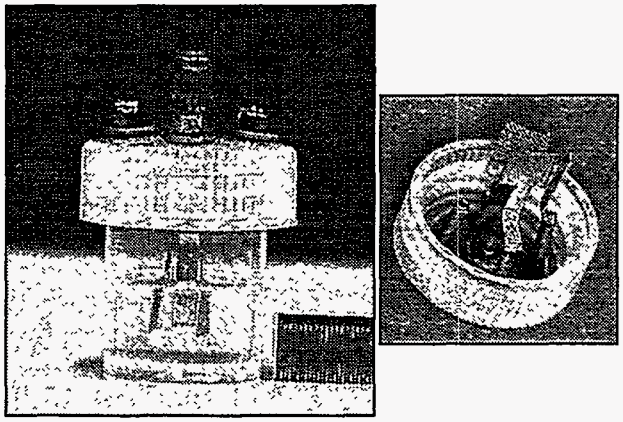

Figure 2. Photographs of the experimental flooded half-cell configuration

In addition to alloy composition, the other parameters that were studied included electrolyte composition, aging (cycling) time, temperature (ambient [22-24 °C], 35°C, 50°C), and initial water content (as received, + 20 ppm). Two electrolyte formulations were used that nominally represented those originally developed by Sony and Bellcore respectively: 1M $LiPF_6$ in either a 1:1 solvent mixture of propylene carbonate and diethylene carbonate (PC:DEC) or in a 1:1 solvent mixture of ethylene carbonate and dimethyl carbonate (EC:DMC). The solvents were purchased from Mitsubishi Chemical and had a maximum water content of 10 ppm. The 20 ppm of additional water was completely miscible in the electrolyte and was added with a micropipette prior to cell assembly. Finally, the effectiveness of two forms of a carbon/fluorocarbon-based coating on improving corrosion behavior was also evaluated. The as-received precursor material was applied to the active face of the aluminum electrode by air brushing. The first coating was produced by curing the sprayed layer for 15 minutes at 120°C. A second coating version involved a similar cure followed by polymerization at 232°C for 10 minutes. The cured coating thickness varied from about 13 μm to 15 μm.

Prior to cell assembly, each aluminum and copper electrode was degreased: the aluminum in a sodium silicate/sodium carbonate solution for 2 minutes at 60°C and the copper in acetone. Following a deionized water rinse, the aluminum samples were then etched in sodium bromate and nitric acid for 2 minutes. The copper electrodes were pickled for 3 minutes in 10% HCl. With the electrodes spot welded in place, the cell was transferred to a glove box for filling. Each

cell was filled with approximately 8 ml electrolyte which ensured the electrolyte would not contact the nickel tab strip. For safety during transport and EIS testing, the cells were placed in lidded glass jars. Wire leads were soldered between the external binding posts on the cell feed-throughs and the binding posts on the caps of the jar. In addition, a small quantity of molecular sieve desiccant was placed in the jars to absorb any moisture present.

Individual cells were aged using a simulated low-earth-orbit (LEO) cycle. Each 150-minute LEO cycle regime consisted of four phases: discharge, constant current charge to voltage cutoff, potentiostatic charge at the voltage cutoff, and dwell (Figure 3). This type of aging simulated the electrical conditions the respective current collectors in an aerospace application might undergo. The relatively high top-of-charge voltage (4.2 V) for the aluminum electrodes was selected as a slight overtest condition (i.e. top-of-charge voltage for a Sony cell is nominally 4.1 V). Electrical cycling was performed by connecting all cells on test in parallel and controlling the voltage on the assemblage with a programmable potentiostat (Figure 4).

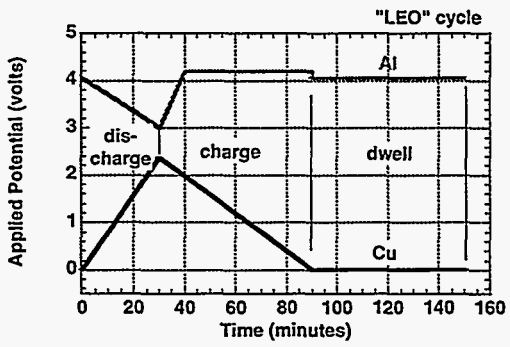

Figure 3. Simulated low-earth-orbit (LEO) electrical cycle regime

Figure 4. Photograph of the Al half cells undergoing LEO cycling

Periodically, cells were taken off LEO cycling to characterize the corrosion kinetics and passivation behavior of the candidate aluminum and copper alloys with electrochemical impedance spectroscopy (EIS). A standard EIS configuration was used. Frequency was scanned from 65 kHz to 10 mHz, and the measurements were conducted either at open circuit (Al and Cu) or 4.2 V versus the lithium reference electrode (Al only). The Al potentials were chosen to measure the response at two extremes that a real battery electrode could encounter. For reference, the EIS technique involves the application of an AC signal of low amplitude via the counter electrode and the analysis of the resultant response. EIS is advantageous because it is non-destructive, can be performed in-situ, yields quantitative information on passivation behavior and corrosion kinetics, and the data can be modeled using equivalent electrical circuits. The presence of a capacitive behavior in these electrochemical systems results in an AC phase shift and an imaginary impedance component. An ideal capacitor has a phase angle shift of 90°, while an ideal resistor has a phase angle shift of 0°. EIS data are typically analyzed using three different graphs. The Nyquist plot is a comparison of the real component of impedance to the imaginary

component. The Bode Magnitude plot, abbreviated Bode |Z|, is a comparison of the applied frequency to the magnitude of the cell impedance. The Bode Phase plot is a comparison of applied frequency to the phase angle. Practically, the Bode |Z| and Bode Phase plots are more useful for data analysis because the important effects of frequency can be easily identified.

The equivalent electrical circuits have discrete elements, such as capacitors and resistors, that can be mathematically deduced from the impedance spectra of many corrosion reactions. The physical meaning of each element helps to identify the actual processes and mechanisms that occur. The study of aluminum corrosion with EIS presents some instrumentation challenges because of the very high inherent resistance of its protective oxide layer and the associated extremely low electrical current.

The corrosion of aluminum with an external coating such as paint or the C-based one used in this study can be modeled using the general circuit shown in Figure 5. Each constituent in the circuit has a corresponding circuit component: solution/electrolyte (R_S), coating, oxide layer, and localized pits. Previous work involving aqueous corrosion of aluminum has shown that the charge transfer resistance through the oxide layer is much greater than that for the charge transport process through the pits in the aluminum [4]. This large R_{oxide} essentially removes the entire oxide RC component from the general circuit, resulting in a less-complex model. Figures 6 and 7 are simplified schematic diagrams that illustrate the dominant processes for uncoated and coated aluminum electrodes, respectively. For aluminum, reasonable empirical mathematical correlations can only be obtained if distributed elements (designated by the >> symbol in Figures 6-7) are substituted for the discrete capacitors used in more general models. Such equivalent circuits have been successfully used to assess the corrosion resistance of chemically passivated Al alloys [4]. Although a distributed element has no physical basis, it behaves mathematically like a "leaky" capacitor. Based on similar experience with aqueous systems, the value of the pitting resistance parameter (R_{pit}) represents a credible figure-of-merit measure for the susceptibility of aluminum to corrosion (i.e., the lower the R_{pit} value, the higher the susceptibility to corrosion). This parameter along with the other elements in the equivalent circuit are calculated from the EIS response.

Environmental Cracking of Copper and Cell Validation

The susceptibility of copper to EAC was assessed using constant extension rate testing (CERT) and exposure of U-bend samples (with actual foil stock) in flooded cells. Photographs of the CERT test apparatus are shown in Figure 8. The strain rates used varied from 10^{-6} to 10^{-7} cm/sec. The CERT experiments were performed on 6.3 mm round copper tensile bar samples (Figure 8a) either at open circuit or near the lithium potential. This latter condition was achieved by either (1) cold welding a strip of lithium onto the copper rod (cell configuration shown in Figure 8b), or (2) by using a Aardvark V-2LR potentiostat, a concentric platinum mesh counter electrode, and a lithium reference electrode in the stainless steel cell shown in Figure 8c. To determine if EAC might occur under more realistic conditions, a number of half cells were constructed and cycled with copper foil electrodes bent into a "U-shaped" configuration. This shape was maintained by spot welding the foil end back onto the body. The radius of curvature was relatively tight at about 0.08 cm to ensure significant plastic deformation.

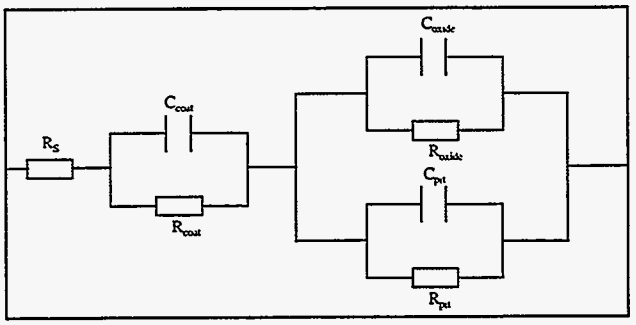

Figure 5. General equivalent circuit model for corrosion of coated aluminum

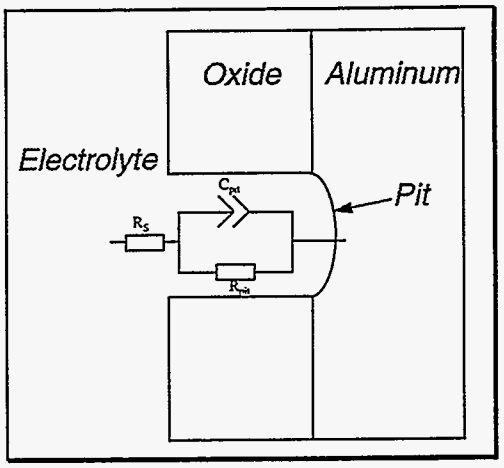

Figure 6. Simplified equivalent electrical circuit representation of the electrochemical processes occurring at the surface of an uncoated aluminum electrode

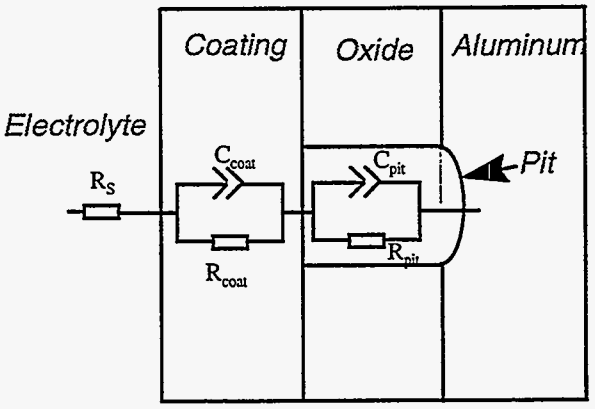

Figure 7. Simplified equivalent electrical circuit representation of the electrochemical processes occurring at the surface of a coated aluminum electrode

For the purpose of validating the results of this study, a portion of the positive-electrode current collector from a heavily cycled (>4000 standard LEO cycles) commercial Sony cell (vintage c.a. 1991) was studied using optical microscopy. To permit this inspection, the active electrode oxide material was dissolved off the aluminum using dimethylformamide.

Surface Analysis

The surface of selected Al 1100 and Cu 110 samples was analyzed using x-ray photoelectron spectroscopy (XPS) and Auger spectroscopy. Analyses were performed on samples obtained directly after initial electrode preparation and cleaning, after static immersion in each electrolyte solution for 64 hours, and after completing approximately 100-200 LEO cycles in cells. In addition, a heavily pitted Al 1100 sample was examined after 690 LEO cycles in the PC:DEC electrolyte. The immersed samples and the electrodes after LEO cycling were removed from the electrolyte, rinsed with the volatile electrolyte solvent component (DEC or DMC), and mounted

onto stainless steel sample stages in the glove box and sealed into glass jars. These samples were transferred into the x-ray photoelectron spectrometer load lock through a plastic glove bag purged with Research Grade He, insuring no direct atmospheric exposure prior to surface analysis. The as-cleaned samples and the heavily pitted sample were not transferred through a glove bag and did experience direct atmospheric exposure prior to surface analysis.

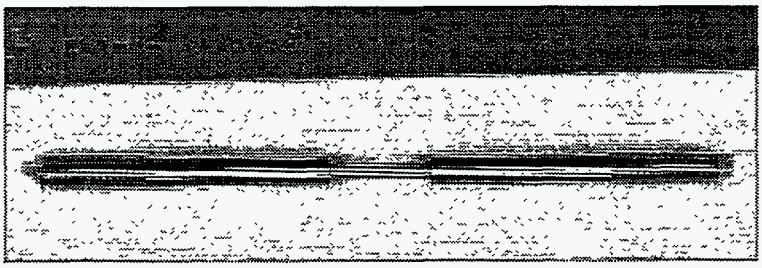

(a)

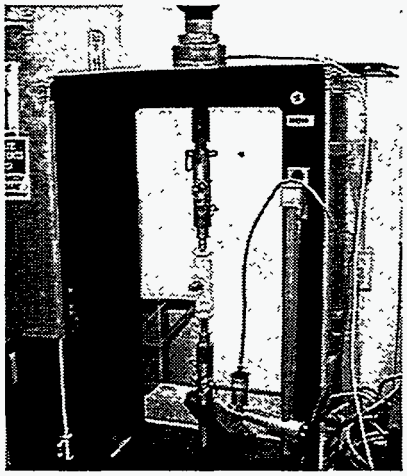

(b)

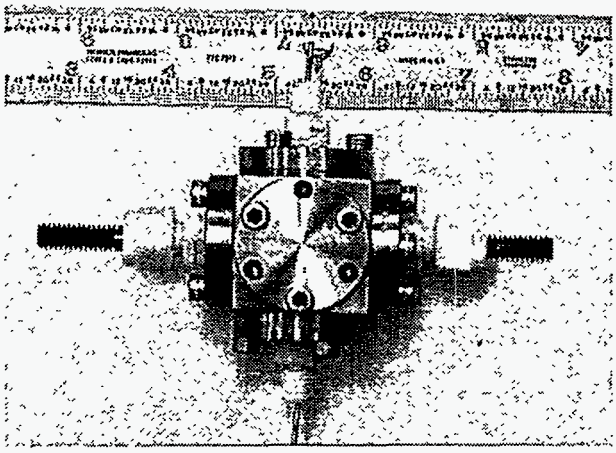

(c)

Figure 8. Photographs of the equipment used to determine susceptibility of copper to EAC: (a) copper tensile bar (alloy 110; diameter = 6.3 mm), (b) the constant extension rate test (CERT) apparatus, (c) stainless steel cell used to conduct constant potential CERT experiments.

All samples were analyzed using a PHI 548/3027 x-ray photoelectron spectrometer with a typical base pressure of 5 x 10^{-10} torr. Spectra were acquired using an Al K_α source (1486.6 eV) at 15 keV and 600 W power. Energy analysis was performed with a double-pass cylindrical mirror energy analyzer (CMA) operated at 50 eV pass energy (100 eV pass energy for Survey spectra) and an average detection angle 47° from the sample surface normal. Survey and high resolution regional spectra were digitally acquired simultaneously by consecutively performing one scan at a time in series for each region. Survey spectra used a 1.0 eV step voltage, while a step voltage of 0.1 eV was used for the high resolution regional spectra. Sampling depths in this mode are typically less than 150 Å and are a function of the energy of the detected electrons.

Each spectrum was digitally processed to calculate surface compositions and reduce the noise and artifacts present in the spectrum. A linear background and contributions arising from extraneous x-ray satellites were subtracted from each spectrum. Each spectrum was then smoothed using a Savitzky-Golay convolution procedure [5,6,7] and peak areas were determined by integrating the area under the respective peaks above the linear baseline. Sample compositions were determined by assuming homogeneous distributions of all observed species across the surface and in depth, using standard handbook sensitivity factors [8]. All surface compositions are reported in atomic percentage values.

Auger spectra were obtained for a heavily pitted Al 1100 sample after 690 LEO cycles in the PC:DEC electrolyte. This sample was analyzed using a PHI 3067 scanning Auger spectrometer with a typical base pressure of 8×10^{-10} torr. Auger point spectra were acquired using a 5 keV electron beam, while Auger maps were acquired using a 256 x 256 point matrix at 50 to 100x magnification and an 8 keV electron beam. Spectra were digitally acquired with the sample normal parallel to the analyzer axis using V/f conversion detection with a single-pass CMA.

RESULTS AND DISCUSSION

Aluminum Corrosion

During electrical cycling, the aluminum current collector undergoes a form of pitting corrosion. After several days of cycling and 40 LEO cycles, some general attack of the aluminum surface was visible in that an almost electropolished appearance existed, but more importantly, some scattered pitting had initiated (compare Figures 9-10). With continued cycling, the pit density increased, as shown in Figure 11 for 690 LEO cycles in the PC:DEC electrolyte. Cycling in the EC:DMC electrolyte resulted in a higher pit density, as shown in Figure 12, even at 150 LEO cycles. Curiously, what optically appeared to be pits after extended cycling in both electrolytes are actually mounds. Based on cross-sectional SEM examination of the foil (Figures 13-14), these mounds must be filled in pits. Surface analyses using XPS and Auger analyses were performed to help understand this phenomenon (detailed results presented below). Initial results indicate that the mounds contain both Al^{o} and Al_2O_3. Because of the primarily anodic conditions during LEO cycling, the existence of metallic aluminum implies that the mounds are electrically isolated from the foil. Two possible explanations are that 1) corrosion and its associated reaction products undermined the surface of a developed pit and caused the overlying metal to bulge and break away, or 2) metal was redeposited on poorly conductive corrosion products during the discharge portion of the LEO cycle during which cathodic conditions actually exist (open circuit voltage for Al is between 3.2 and 3.6 V).

The results from the electrochemical impedance spectroscopy measurements provide insight and understanding into the Al corrosion processes. First, as discussed above, pit density is higher in the EC:DMC electrolyte. The EIS results (Figures 15-16) confirm that the EC:DMC electrolyte is more corrosive (lower R_{pit}) than the PC:DEC electrolyte over the majority of the tested cycle life. At cycle 100, the diameter of the semicircular component in Figure 15 that corresponds to R_{pit} is much smaller and, as shown in Figure 16, a distinct separation in the explicitly calculated R_{pit} values from the model exists over the first several hundred cycles. The increased corrosion

current observed initially during DC measurements also support this conclusion (Figure 17). Second, and importantly, the pitting resistance appears to improve with cycling in both electrolytes, but especially in the EC:DMC solvent (Figure 16). However, as discussed below, this does not mean that the pitting process is self-limiting over time and stops in either electrolyte. Also note that no attempt was made to analyze impurities and then monitor changes during cycling in either electrolyte. As such, these differences may not be an intrinsic property and could be due to an associated impurity effect. Preliminary surface spectroscopy results (again see Surface Analysis section) indicate that the EC:DMC electrolyte used in this study may have had a higher chloride concentration, which is known to cause pitting corrosion in organic electrolytes [9].

Using electrochemical response and R_{pit} as a measure of corrosion susceptibility, the general effects of the other environmental parameters are summarized as follows:

- General electrochemical behavior is not substantially affected by cycling in either electrolyte (EIS in Figures 18 and 19 and DC in Figure 20). The removal of the secondary peak in the PC:DEC DC polarization response (Figure 20) that occurs during early cycling is probably due to an one-time irreversible reaction involving an electrolyte impurity.
- The greater the applied anodic voltage the greater the anodic corrosion current (Figure 20), a result consistent with a lower R_{pit} value (smaller semi-circle diameter in the Nyquist plot shown in Figure 21).
- The metallurgical purity of the electrode material (alloy 1145 vs. 1100) does not have a substantial effect on the resistance to pitting in the PC:DEC electrolyte (Figure 22).
- The addition of 20 ppm water to the PC:DEC electrolyte appears to substantially improve corrosion resistance after 100+ cycles (Figure 23). A similar beneficial effect due to water (although at much higher levels) has been observed in a related work that involved a PC-based electrolyte and stainless steel couple. The effect was attributed to a stabilizing effect on the passive layer [10]. However, a more detailed analysis is needed with this system before a definitive conclusion can be reached. Of possible relevance to this understanding and confirmed by the DC response obtained during LEO cycling, the water appears to be effectively electrolyzed out during the first few LEO cycles (Figure 24). Possibly, a chemical radical product during the electrolysis is an effective passive-layer stabilizer.
- The attempt to accelerate aging using higher temperature with the PC:DEC electrolyte was not successful because the electrolyte was not stable at either the mid (35°C) or the high (50°C) level. Of note, the cells were simultaneously subjected to the relatively high LEO charge voltage. After only 32 cycles at 35°C and only 7 at 50°C, the electrolyte had turned black and dissolved the Li reference electrode.

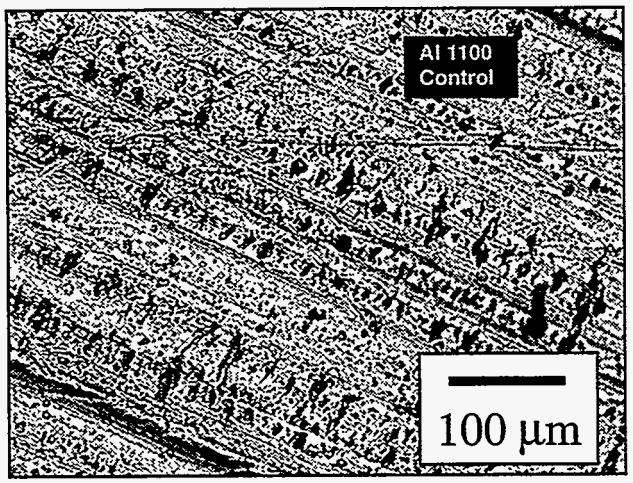

Figure 9. Photograph of the bare Al surface prior to LEO cycling

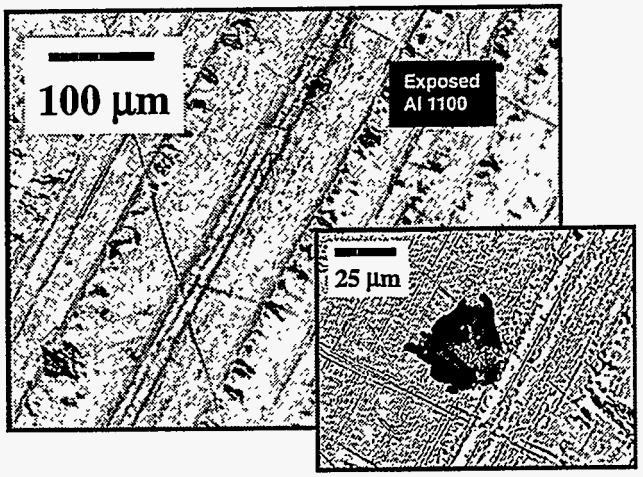

Figure 10. Photographs of the Al surface after 40 LEO cycles in PC:DEC electrolyte

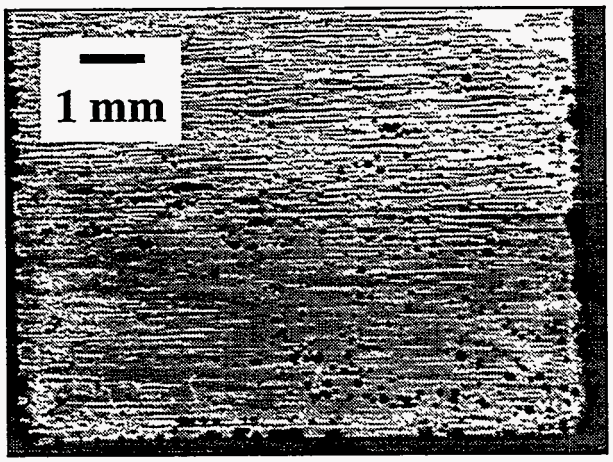

Figure 11. Photograph of an Al surface after 690 LEO cycles in PC:DEC electrolyte

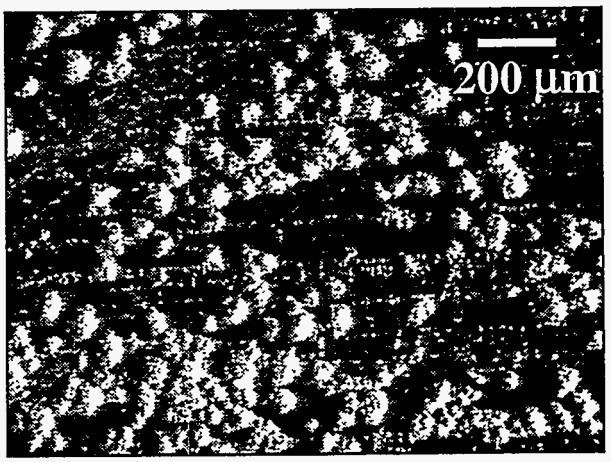

Figure 12. Photographs of the Al surface after 150 LEO cycles in EC:DMC electrolyte

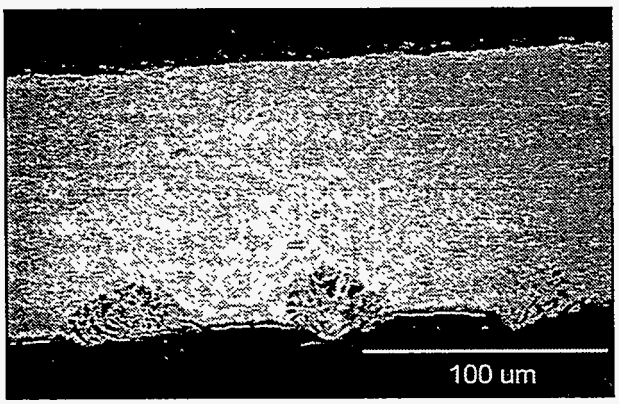

Figure 13. SEM cross-section of Al foil after 150 cycles in EC:DMC electrolyte

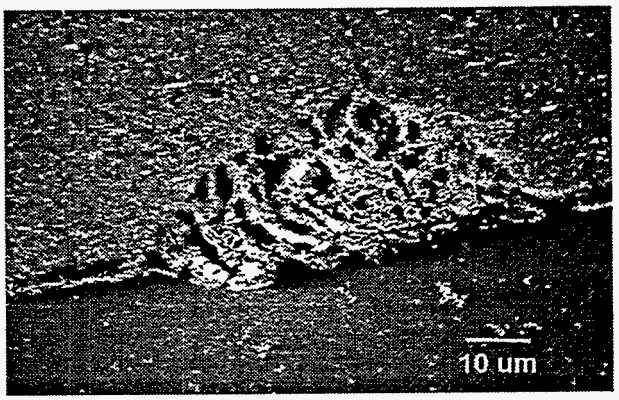

Figure 14. SEM cross-section of Al foil after 150 cycles in EC:DMC electrolyte (expanded view of one mound from Figure 13)

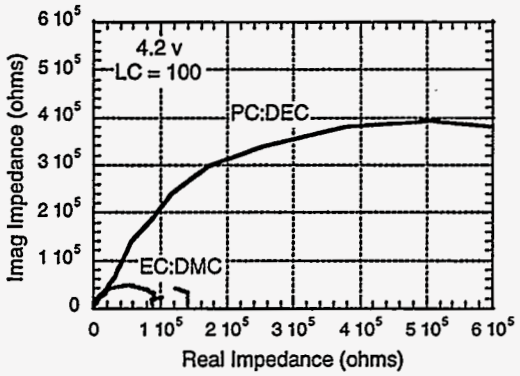

Figure 15. Nyquist plot for Al alloy 1100 in PC:DEC and EC:DMC electrolytes

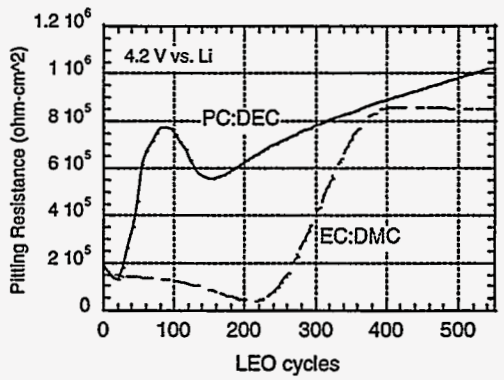

Figure 16. Effect of cycling on the calculated R_{pit} parameter for both electrolytes (Al 1100)

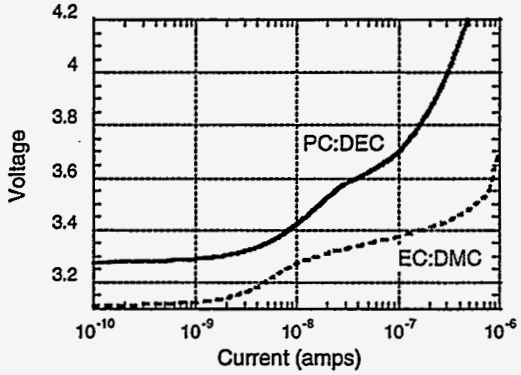

Figure 17. Comparison of anodic DC polarization response for Al alloy 1100 in PC:DEC and EC:DMC electrolytes prior to cycling

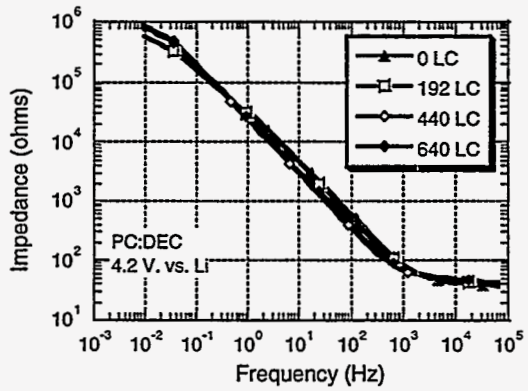

Figure 18. Bode magnitude plot for aluminum alloy 1100 in PC:DEC electrolyte

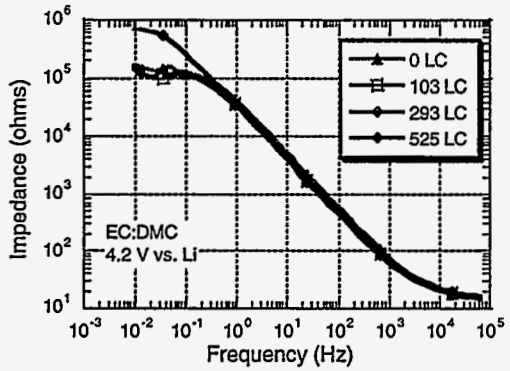

Figure 19. Bode magnitude plot for aluminum alloy 1100 in EC:DMC electrolyte

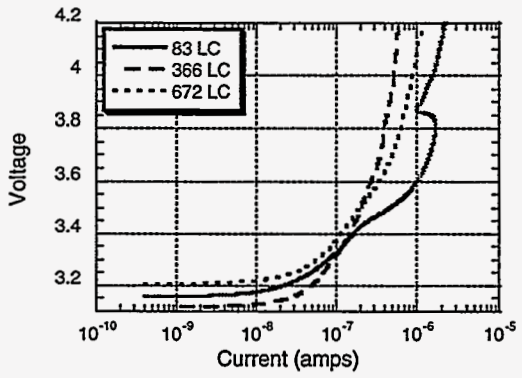

Figure 20. Anodic DC polarization response for Al alloy 1100 in PC:DEC electrolyte as function of cycling

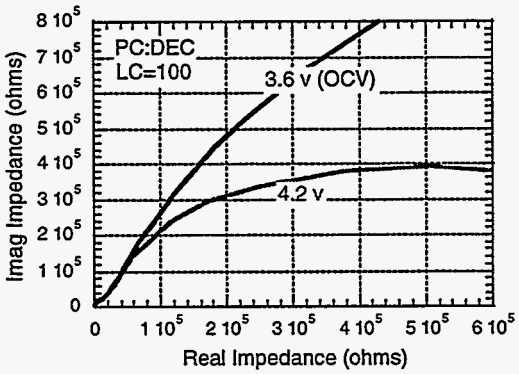

Figure 21. Nyquist plot for aluminum alloy 1100 in PC:DEC electrolyte (at 2 voltages)

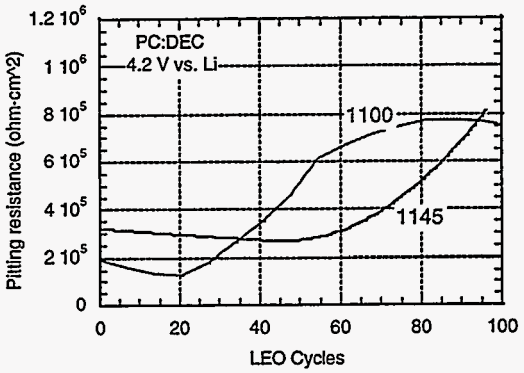

Figure 22. Effect of alloy composition on the calculated R_{pit} parameter in PC:DEC electrolyte

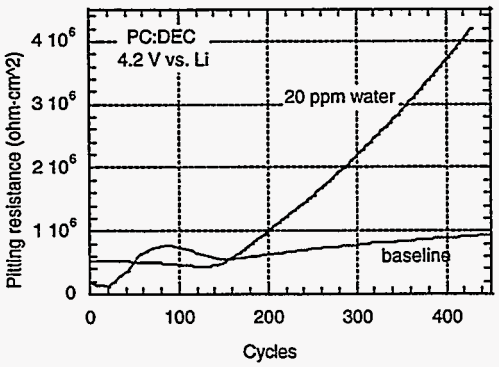

Figure 23. Effect of an initial water addition on the calculated R_{pit} parameter for Al alloy 1100 in PC:DEC electrolyte.

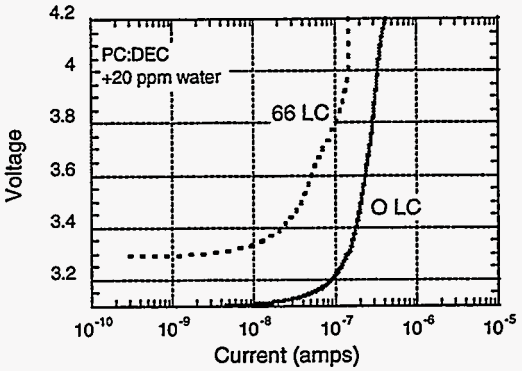

Figure 24. Anodic DC polarization response for Al alloy 1100 in PC:DEC electrolyte into which 20 ppm H_2O was initially added

The effect of the two carbon-based coatings on the general electrochemical behavior of Al is depicted in the Bode phase plot shown in Figure 25. The uncoated electrode has a single dominant process (represented with a single capacitive/resistive combination and thus one pseudo-time constant), whereas the two coated electrodes show two processes: the non-polymerized with two overlapping time constants, and the polymerized with two distinct time constants. Modeling results for EIS data taken around LEO cycle 100 are shown separately in Figures 26-28 for a bare electrode and the two coated electrodes. The two lines in each plot demonstrate the favorable comparison between the modeling predictions and the actual data. The low frequency limit results indicate that pitting resistance can increase by close to one order of magnitude for coated electrodes. The higher resistivities for the coated electrodes implies that less corrosion should be present. This prediction is confirmed by the photograph presented in Figure 29 (compare with Figure 11 for uncoated Al). As shown in Figure 30, some interaction (swelling and delamination) did occur between the electrolyte and both coatings, yet protection

was still provided. As such, the ability to provide long-term protection is unknown. Although not confirmed with surface analysis, a possible reason that these coatings improve the corrosion resistance of aluminum is that much of the active pit area becomes sealed.

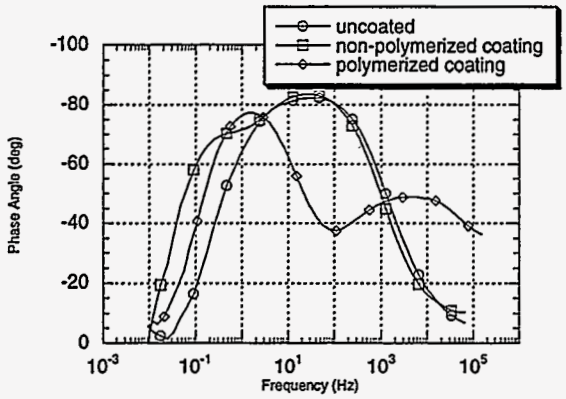

Figure 25. Bode phase plot for uncoated and coated aluminum electrodes

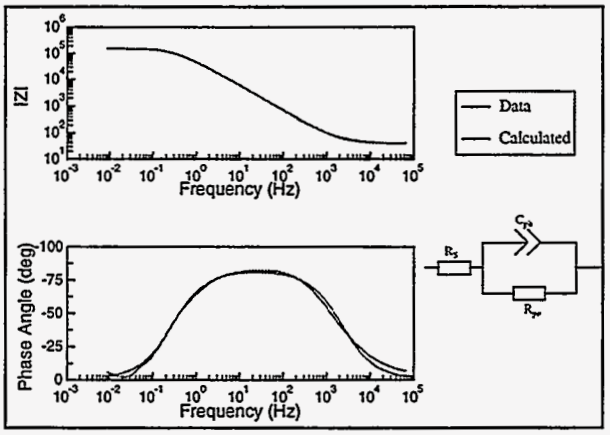

Figure 26. Bode plots for the uncoated aluminum electrode in the PC:DEC electrolyte.

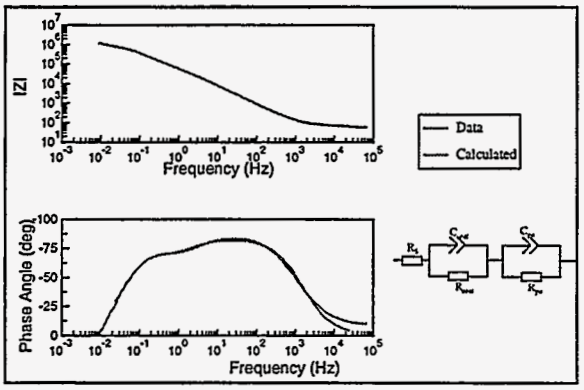

Figure 27. Bode plots for non-polymerized C-coated Al in PC:DEC electrolyte

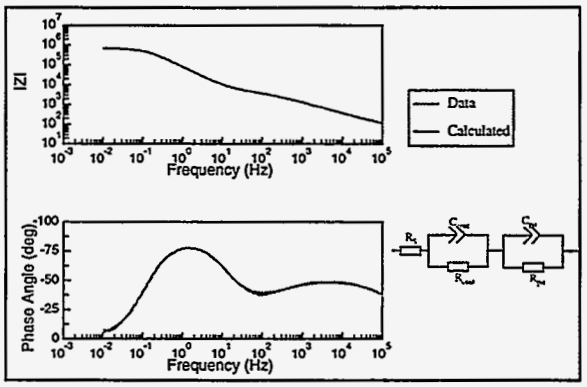

Figure 28. Bode plots for polymerized C-coated Al in the PC:DEC electrolyte

A practical validation of these results comes from a section of a positive electrode taken from a commercial Sony Li-Ion cell (1991 vintage) that had been subjected to about 4000 LEO cycles. Two representative photographs are shown in Figures 31 and 32. Significant localized pitting corrosion of the aluminum occurred to the point that the foil had a large number of visible perforations. Whether or not the holes were at some time mounds is presently unknown because of the difficult nature of removing the active materials without physical disruption of the surface. However, this does prove that the pitting process is not self-limiting. An assessment of the final resistivity of the foil has not been made to determine if the limited general corrosion had a significant effect on cell resistance. However, such a measurement would be meaningless without the corrosion products in place, a situation that cannot be ensured with extracted electrodes such as these.

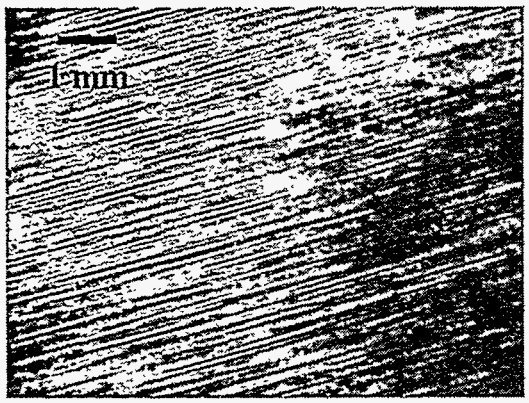

Figure 29. Al substrate after polymerized C coating removed after 445 cycles

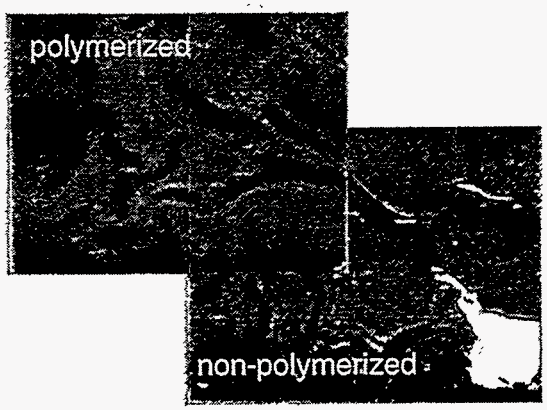

Figure 30. Polymerized and non-polymerized coatings after 445 LEO cycles

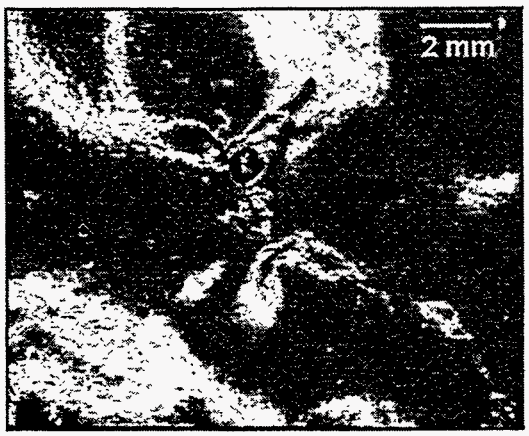

Figure 31. Al current collector from commercial Sony cell after 4000 LEO cycles

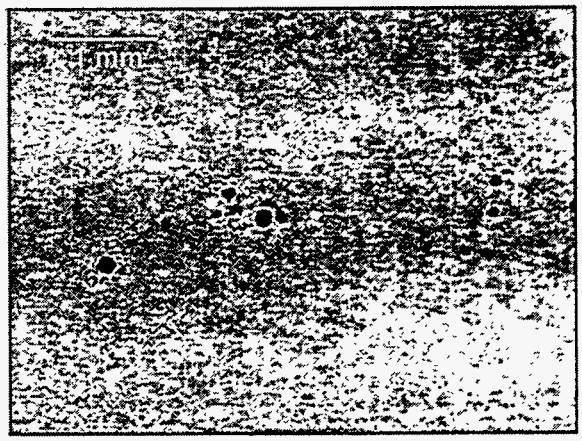

Figure 32. More detail of current collector shown in Figure 31

Copper Corrosion

As expected and shown in Figures 33 and 34, copper is not attacked at the cathodic potentials associated with actual cells. That is, copper has an open circuit voltage in these electrolytes that is > 3 V vs. Li and the "applied" potential on the electrode ranges from about 0 V to ~1.5 V vs. Li. The conditions studied were similar to those described above for aluminum: baseline, initial water addition of 20 ppm, two carbon coatings, and temperature. As with aluminum, elevated temperature led to premature breakdown of the electrolyte. However, and probably due to the lower applied voltage, the onset of degradation was much longer (> 100 LEO cycles). Although not tested with aluminum, the EC:DMC formulation showed better high temperature longevity. Typical EIS results are shown in Figures 35 and 36. In general, no conditions were found that resulted in either uniform or localized attack of the copper. The presence of the two carbon coatings also had no effect.

Figure 33. Photograph of the bare copper surface prior to LEO cycling

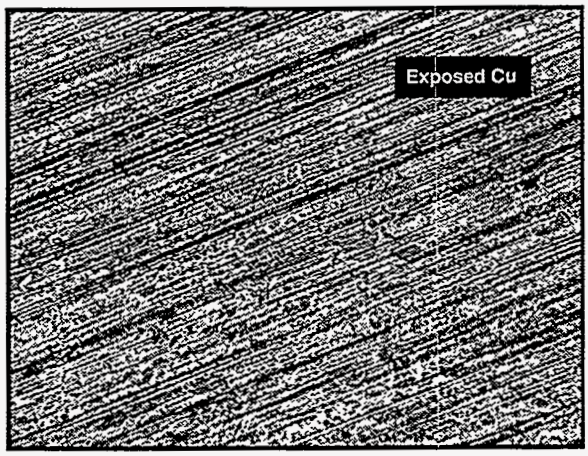

Figure 34. Photographs of the copper surface after 40 LEO cycles in PC:DEC electrolyte

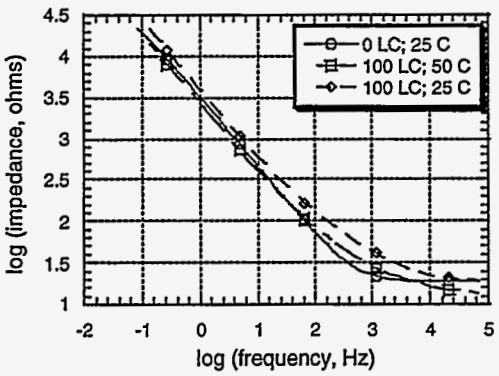

Figure 35. Effect of cycling on the Bode magnitude response for Cu alloy 110 cycled in PC:DEC electrolyte (cycling at 50 C; measurement temperature indicated)

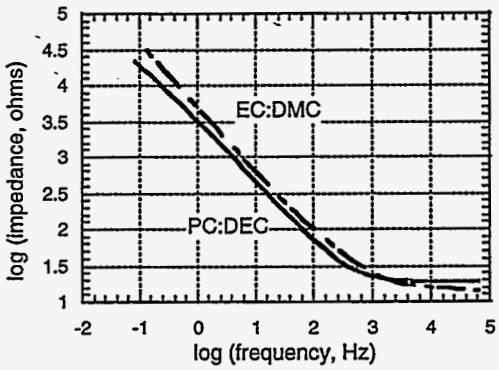

Figure 36. Comparison of Bode magnitude response for Cu alloy 110 in PC:DEC and EC:DMC electrolytes prior to LEO cycling

Surface Analysis

An important part of this study involved a detailed analysis of the passivating films that form on the aluminum and copper current collectors. Because organic solvents are used in the Li-Ion technology, conventional aqueous knowledge is not applicable. The primary characterization techniques used in this study included x-ray photoelectron spectroscopy (XPS) and scanning Auger microscopy (SAM).

Figures 37 to 41 show selected comparisons of the observed surface compositions as measured by XPS. All compositions reported in these tables and their corresponding figures are in atomic percentages. Li is the predominant elemental species observed on the surface of all electrodes. However, the surface layer is not simply adsorbed electrolyte. In general, about twice as much F is observed on the surface than would be associated with the deposition of $LiPF_6$. The existence

of non-stoichiometric decomposition products suggests that some decomposition of the electrolyte solution is occurring. In addition, higher pitting and corrosion appears to correlate with increased surface concentrations of Cl, presumably present as a contaminant in the electrolyte solutions. This peak could possibly be associated with B instead of Cl. Cl and B are usually distinguished from each other by the relative binding energies (BE) of the peak. However, in this work, the observed BE fell between that expected for Cl and B, and thus a definitive identification could not be made.

Figure 37 (Al 1100) and Figure 38 (Cu 110) show the comparison of surface compositions for samples after initial electrode preparation and cleaning, after immersion in the PC:DEC formula electrolyte for 64 hours, and after completing LEO cycling (212 cycles for Al, 100 for Cu) in cells containing the PC:DEC formula electrolyte. There is very little difference observed for immersion in the electrolyte versus actually cycling the cell for either electrode material. Cycling the cell produces more Li and less F on the surface, relative to immersion in the electrolyte, while the surface concentrations of other species are essentially unchanged. For every copper sample, including those from cycled cells, the surface layers remain quite thin - well below the 150 Å maximum sampling depth of XPS (as evidenced by the presence of the underlying electrode metal). The situation regarding the thickness of the aluminum is not clear at this point. More aluminum exists in the air-formed oxide layer than in the samples exposed to the electrolytes. But, because the composition of Al is not affected by aging in these cell environments, either the thickness does not change or the composition of the layer is constant. More detailed sputter depth profiling must be performed to clarify this situation. Also, spurious contaminants can be observed after cell cycling, including Cu, Ni and Mn. Many of the differences observed for the samples after initial electrode preparation and cleaning may be attributed to the fact that these samples were not transferred into the XPS system through the glove bag, but were exposed to laboratory air prior to analysis. Very few differences are observed between the Al 1100 and Cu 110 electrode surfaces. Prior to placement in the cells, after initial electrode preparation and cleaning, the Al surface shows higher O and lower C, relative to the Cu surface. Immersion in the electrolyte produces much greater surface concentrations of Li and slightly lower concentrations of F, O, C and P for the Al surface, relative to the Cu surface. Cycling the cell removes most of the observed differences between the Al and Cu surface compositions.

A comparison of surface compositions for Al 1100 electrodes after completion of a limited number of LEO cycles in cells containing the PC:DEC (212 cycles) versus the EC:DMC (150 cycles) electrolyte is shown in Figure 39. The surface of the Al electrodes are very similar when cycled in a cell containing either PC:DEC or EC:DMC formula electrolytes, suggesting that the common $LiPF_6$ electrolyte salt has the dominant effect. The primary difference observed is an increase in Cl (possibly B) in the EC:DMC formula electrolyte relative to the PC:DEC formula electrolyte.

The surface compositions for uncoated and non-polymerized carbon-coated Al 1100 electrodes after LEO cycling in cells containing the PC:DEC formula electrolyte are presented in Figure 40. Carbon coating of the Al electrode produces a surface which has increased C and decreased F and Li, relative to the uncoated Al electrode. The carbon-coated electrode also show lower contaminant (Cu, Cl) concentrations, relative to the uncoated electrode. Most surface species

show multiple or broadened peaks on the carbon-coated Al electrode, which is evidence of multiple types of chemical species present on the surface. As noted above for other Al electrode surfaces, the presence of the Al electrode substrate material is observed, even for the carbon-coated electrode. Since the known carbon film thickness is far in excess of the 150 Å maximum sampling depth of XPS, the carbon film must be highly porous in order to continue to observe significant substrate species through the coating.

Al	Na	Zn	Cu	F	O	N	Ca	C	Cl	S	Al	Li	Si	P
Clean	0.4	0.3	0.0	2.1	37.1	1.2	0.7	34.4	0.0	0.3	14.3	0.0	7.3	2.0
Immersed	0.1	0.0	0.0	33.4	6.2	0.2	0.1	6.6	0.6	0.0	3.3	44.5	3.7	1.3
Cycled	0.0	0.0	0.9	23.6	5.6	0.2	0.0	10.9	0.8	0.0	4.2	50.4	2.0	1.5

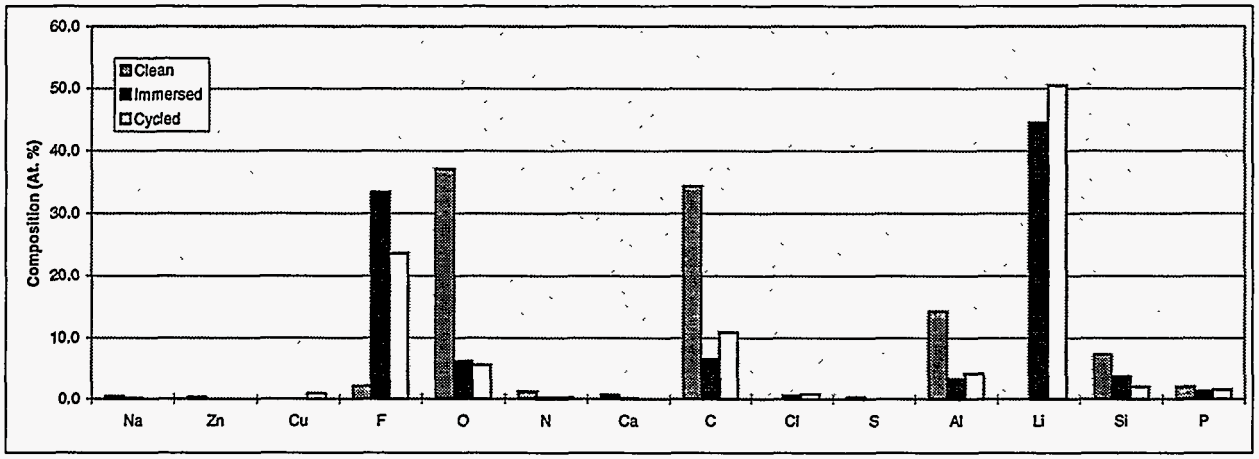

Figure 37. XPS results from analysis of uncoated aluminum exposed to the PC:DEC electrolyte. Composition is in atomic %. The cycled electrode experienced 212 LEO cycles.

Cu	Na	Zn	Cu	F	O	N	Ca	C	Cl	S	Al	Li	Si	P
Clean	0.1	0.1	10.0	0.9	22.9	2.1	0.0	56.0	1.8	0.5	0.0	0.0	3.4	2.3
Immersed	0.3	0.1	3.3	35.7	9.7	0.8	0.0	14.0	1.9	0.0	0.0	27.7	3.9	2.7
Cycled	0.0	0.0	6.5	24.1	9.8	0.3	0.0	8.8	1.4	0.0	0.0	45.5	0.0	3.6

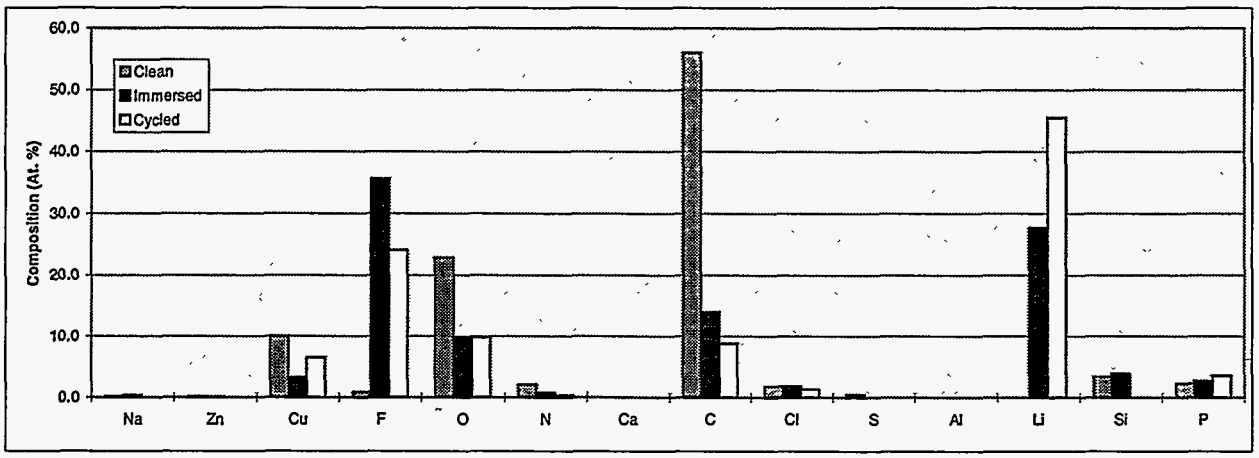

Figure 38. XPS results from analysis of uncoated copper exposed to the PC:DEC electrolyte. Composition is in atomic %. The cycled electrode experienced 100 LEO cycles.

Al	Na	Zn	Cu	F	O	N	Ca	C	Cl	S	Al	Li	Si	P
PC:DEC	0.0	0.0	0.9	23.6	5.6	0.2	0.0	10.9	0.8	0.0	4.2	50.4	2.0	1.5
EC:DMC	0.0	0.0	0.0	24.8	5.8	0.0	0.2	9.9	5.9	0.0	5.2	45.9	0.7	1.7

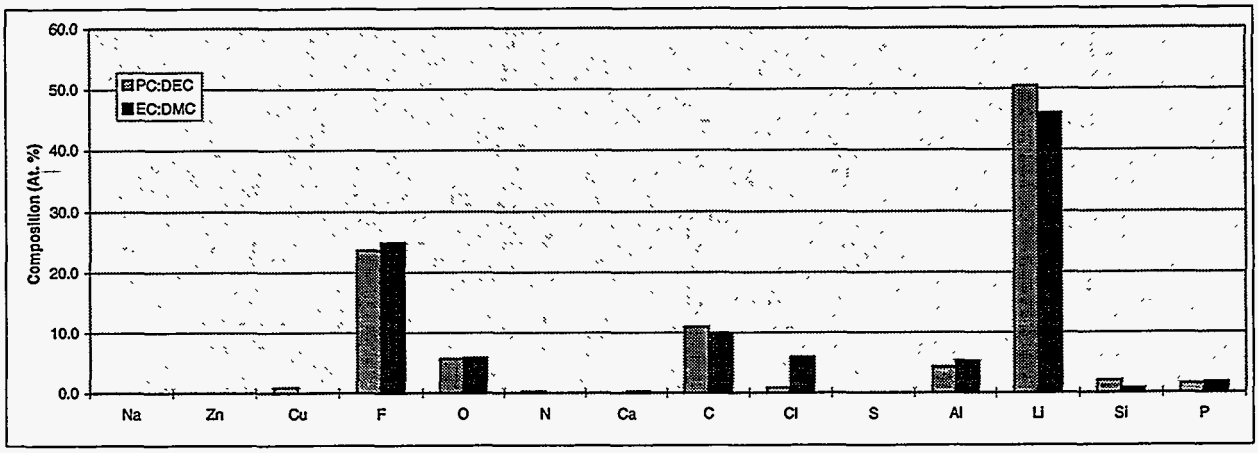

Figure 39. XPS results comparing the surface composition of aluminum after cycling in the PC:DEC electrolyte (212 cycles) and the EC:DMC electrolyte (150 cycles). Composition is in atomic %.

Al	Na	Zn	Cu	F	O	N	Ca	C	Cl	S	Al	Li	Si	P
Uncoated	0.0	0.0	0.9	23.6	5.6	0.2	0.0	10.9	0.8	0.0	4.2	50.4	2.0	1.5
C-coated	0.0	0.0	0.4	20.0	6.6	1.2	0.0	28.9	0.3	0.0	3.1	37.8	0.9	0.9

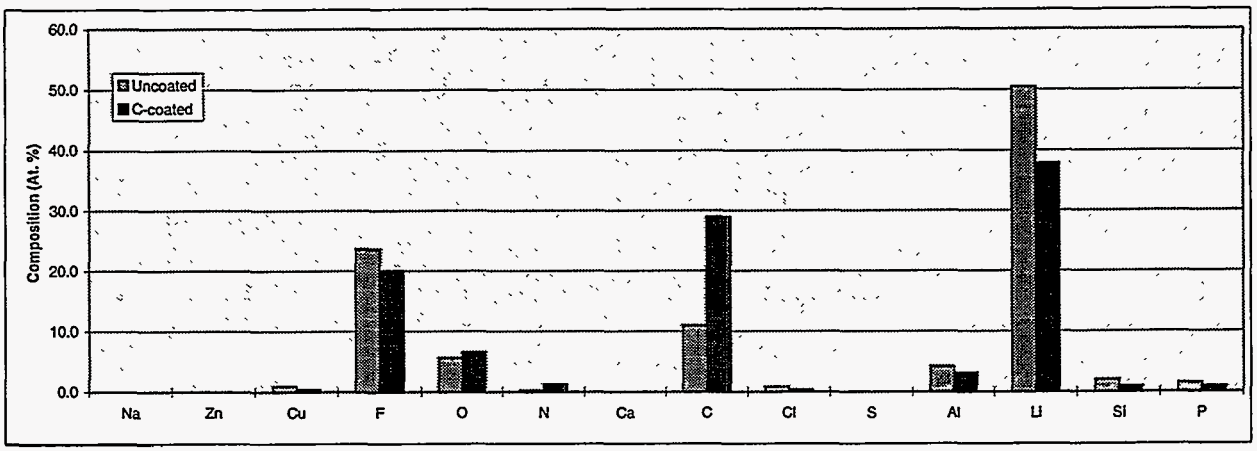

Figure 40. XPS results comparing the surface composition after cycling in the PC:DEC electrolyte of uncoated (212 cycles) and carbon-coated (115 cycles) aluminum. Composition in atomic %.

Figure 41 shows the comparison of surface compositions for Al 1100 electrodes after completion of 212 and 690 LEO cycles in cells containing the PC:DEC formula electrolyte. The heavily pitted electrode (690 cycles) shows considerably less F and Li and considerably more O, Cl (B?), P and contaminants (Ni, Mn), relative to the unpitted electrode (212 cycles). The source of the contaminants is presently unclear.

Al	Na	Zn	Cu	F	O	N	Ca	C	Cl	S	Al	Li	Si	P	Ni	Mn
212 cycles	0.0	0.0	0.9	23.6	5.6	0.2	0.0	10.9	0.8	0.0	4.2	50.4	2.0	1.5	0.0	0.0
690 cycles	0.1	0.0	0.1	10.0	23.1	0.5	0.4	13.5	3.6	0.0	8.9	25.4	0.5	7.8	4.3	1.9

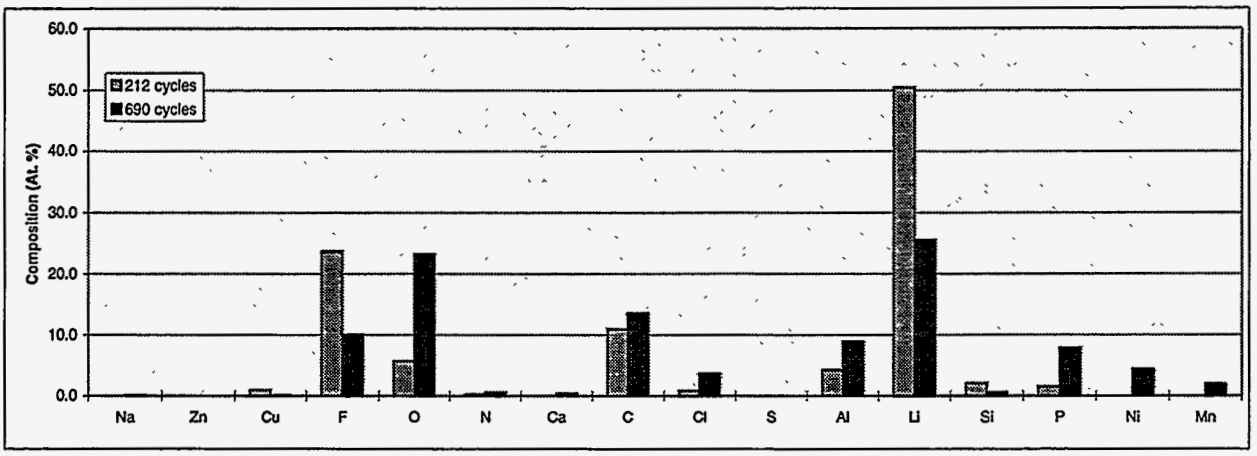

Figure 41. XPS results comparing the aluminum surface composition from short-term cycling (212 cycles) and long-term cycling (pitted - 690 cycles) in the PC:DEC electrolyte. Composition in atomic %.

Most of the surface species contain the same chemical state regardless of cell processing (immersion versus cycling, electrolyte composition), with minor differences observed for Al surfaces relative to Cu. The exception is the carbon-coated surface, which shows multiple peaks and chemical states for surface species, some quite different from those observed on the other surfaces. These observations are illustrated in Figure 42 that consists of selected regional spectral plots for Al 1100 electrode surfaces as a function of cell processing and exposure.

Figure 42a is the XPS regional plot for Li 1s. The peaks for electrodes simply immersed in the PC:DEC electrolyte formula and those after completion of 150-20 LEO cycles in either electrolyte formula are very similar, with a BE near 59 eV. This BE is very high, suggesting the Li is present in a environment that is extremely electron-withdrawing. Representative BE values for species such as LiF, LiOH and Li_2O are all near 55 eV [11]. A small shoulder is observed in all of the spectra near the 55 eV peak expected for these type of species. Presently, the likely chemical species present for the Li has not been identified. The carbon-coated electrode as well as the pitted electrode after completion of 690 LEO cycles in the PC:DEC electrolyte formulation show considerably less Li. The chemical state of the Li present on the carbon-coated electrode is quite similar to the other electrodes observed, while the Li present on the pitted electrode occurs at an even higher BE yet, near 60 eV.

Figure 42b shows the XPS regional plots for F 1s. As with the Li region, the peaks for electrodes immersed and cycled for a short time are quite similar, with a BE near 688.5 eV. This BE is typically observed for $-CHF_2$ species [11]. No reference BE for PF_6 has been found yet, but it may very well be near this BE, since the BE for SF_6 is near 693 eV [12]. This BE is quite different from that expected for metal fluorides, which typically occur near 685 eV [11]. The pitted electrode shows considerably less F, which is a slightly broader peak showing evidence of

a primary peak near 688.5 eV, similar to the other electrode surfaces, but also containing a small peak nearer to 690 eV. The carbon-coated electrode also shows much less F, with a broad peak centered near 692.5 eV. This BE is considerably higher than that observed on the other electrode surfaces, suggesting a much more electron-withdrawing environment. Polymer $(CF_2)_n$ chains and highly fluorinated species like $-CF_3$ are more typical of this BE [11]. This peak may be primarily representative of the fluorinated polymer base utilized to form the carbon coating on the electrode.

Figure 42c shows the XPS regional plots for P 2p. The similar peaks exhibited by the immersed and short-term cycled electrodes show a BE near 138 eV. This BE is typical of PF_6^- species [11]. The pitted electrode shows considerably more P, with a BE near 137 eV. While this BE is lower than that on the other electrode surfaces, suggesting P present in a more electron-donating environment, it is still within range of that expected of PF_6^- species [11]. The carbon-coated surface shows almost no P present, but the peak occurs at a BE near 140 eV, suggesting a more electron-withdrawing environment.

Figure 42d shows the XPS regional plots for Al 2p. Although not presented, the original air-formed film on the aluminum is consistent with a thin layer of Al_2O_3. The similar peaks exhibited by the immersed and short-term cycled electrodes show a BE near 78 eV. This BE is high for typical Al species - higher than that expected for Al_2O_3 (74 eV) or AlF_3 (76.5 eV) [11]. The higher BE again indicates the presence of an electron withdrawing environment. The carbon coated electrode shows less Al, with a general shift of intensity to lower BE's more typical of Al_2O_3 and AlF_3. This situation could result simply from the presence of an effective coating over the original air-formed oxide layer. The pitted electrode surface shows a doublet peak, with a small peak near 78 eV similar to the other electrode surfaces and a larger peak near 71 eV which is more typical of Al^0 [11].

XPS regional plots are not shown for other elements, but are typical of those shown. The C 1s region shows a doublet primary peak near 287 eV, typical of adventitious hydrocarbon and oxygenated hydrocarbon species for all electrodes except the carbon-coated electrode [11]. The electrode cycled in the EC:DMC formula electrolyte shows an additional small peak near 292 eV, typical of chlorinated or fluorinated hydrocarbons [11]. The carbon-coated electrode shows a typical fluorinated polymer spectrum, with major peaks near 284, 289 and 296 eV, representative of $-CH_3$, $-CH_2F$ and $-CF_3$ type species [11]. The Cl 2p region shows a primary peak near 195 eV for the immersed and short-term cycled electrodes. This BE is much lower that that expected for typical Cl species, with the only known species exhibiting similar BE levels to be R_4NCl at 196 eV [11]. This BE is also representative of B species like $NaBF_4$ at 195 eV [11]. With the data presently available, this peak cannot be distinguished or unambiguously assigned. The pitted electrode shows a larger peak a slightly lower BE near 194 eV, again unassigned at this time. The carbon-coated electrode shows a small peak near 198 eV, typical of the BE expected for metal chlorides [11]. The O 1s region shows peaks near 534.5 eV for all electrodes except the carbon-coated electrode. This BE is probably best assigned to $Al(OH)_3$ [11]. The carbon-coated electrode shows a doublet peak, with the major peak near 532 eV and a smaller peak near 537 eV. The lower BE peak is typical of Al_2O_3, carbonates and phosphates while the higher BE peak may represent trapped adsorbed H_2O in the carbon film [11].

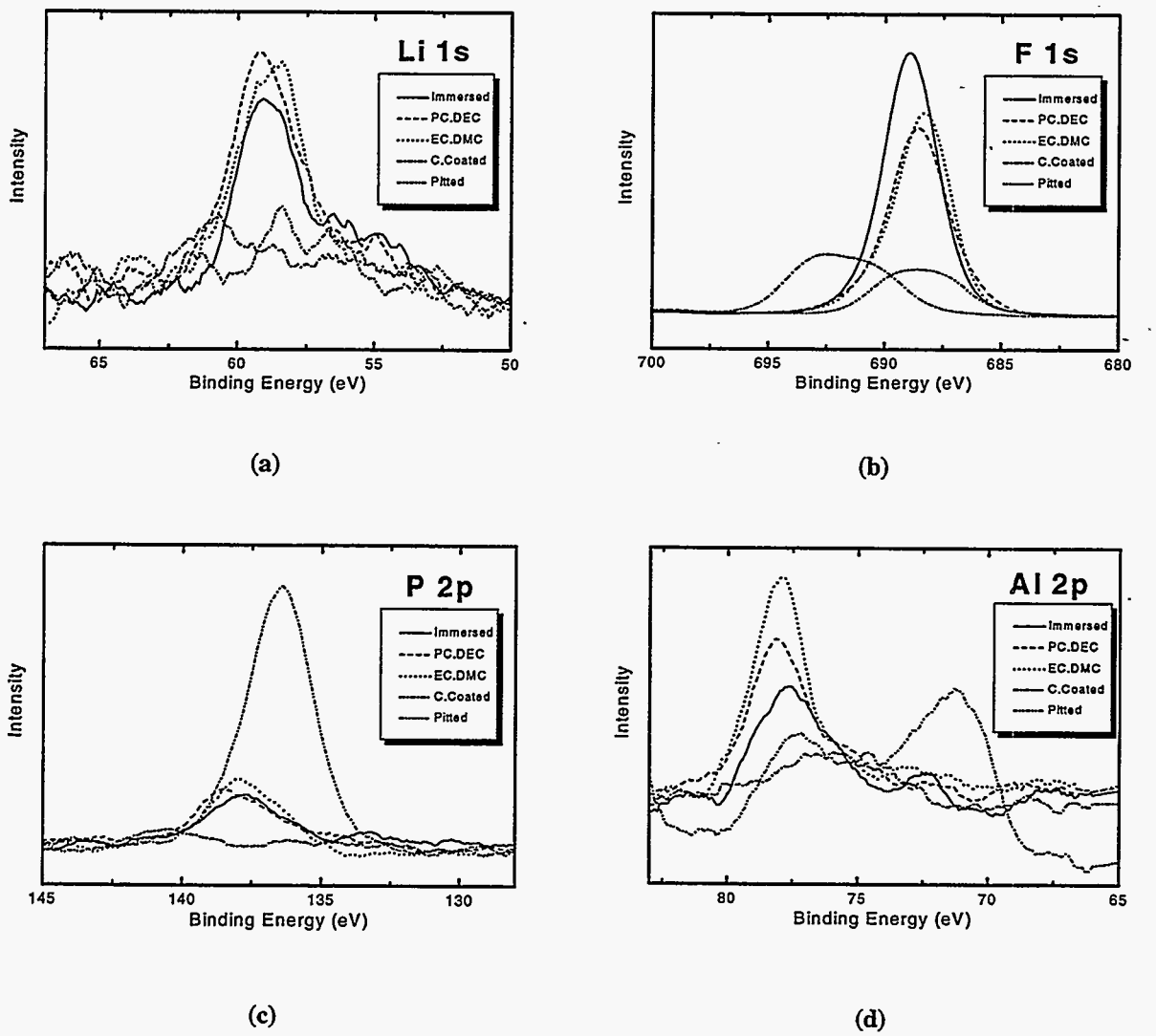

Figure 42. XPS region plots for several elements lithium as a function of exposure conditions for an Al 1100 electrode surface: (a) lithium, (b) fluorine, (c) phosphorus, (d) aluminum. All exposures were in the PC:DEC electrolyte except for the one marked EC:DMC. The Leo cycle number for each are as follows: immersed - 0; PC:DEC - 212; EC:DMC - 150; carbon coated - 115; pitted - 690.

Auger spectroscopy shows that the nodules formed in the corrosion pits on the Al electrode surfaces after long-term cycling have very complex chemistry that varies from nodule to nodule. Point mode Auger spectra taken at selected points on nodules and other general locations of the electrode surface show great inhomogeneity on the microscopic spatial level, but the species observed agree well with those observed by XPS. No specific surface compositions are reported because of quantitative errors caused by local charging effects in many of the locations as a result of the presence of electrically insulated regions, in agreement with the previously described electrochemical assessments. Representative Auger maps are shown in Figure 43 for a portion of the electrode surface at 100x magnification. In general, the nodules show high concentrations of Al, Li and F and also contain Al_2O_3. Al^0 and Al^{+3} are readily distinguished in the Auger spectra based upon differences in the lineshape caused by chemical state, although this assignment may

be complicated by the presence of both electrically conducting and insulating regions within the nodules. Some nodules are high in Cu and P. No clear determination of nodule composition relative to the general electrode surface is possible at this time because of the complexities of the nodule composition and the difficulties with localized charging effects.

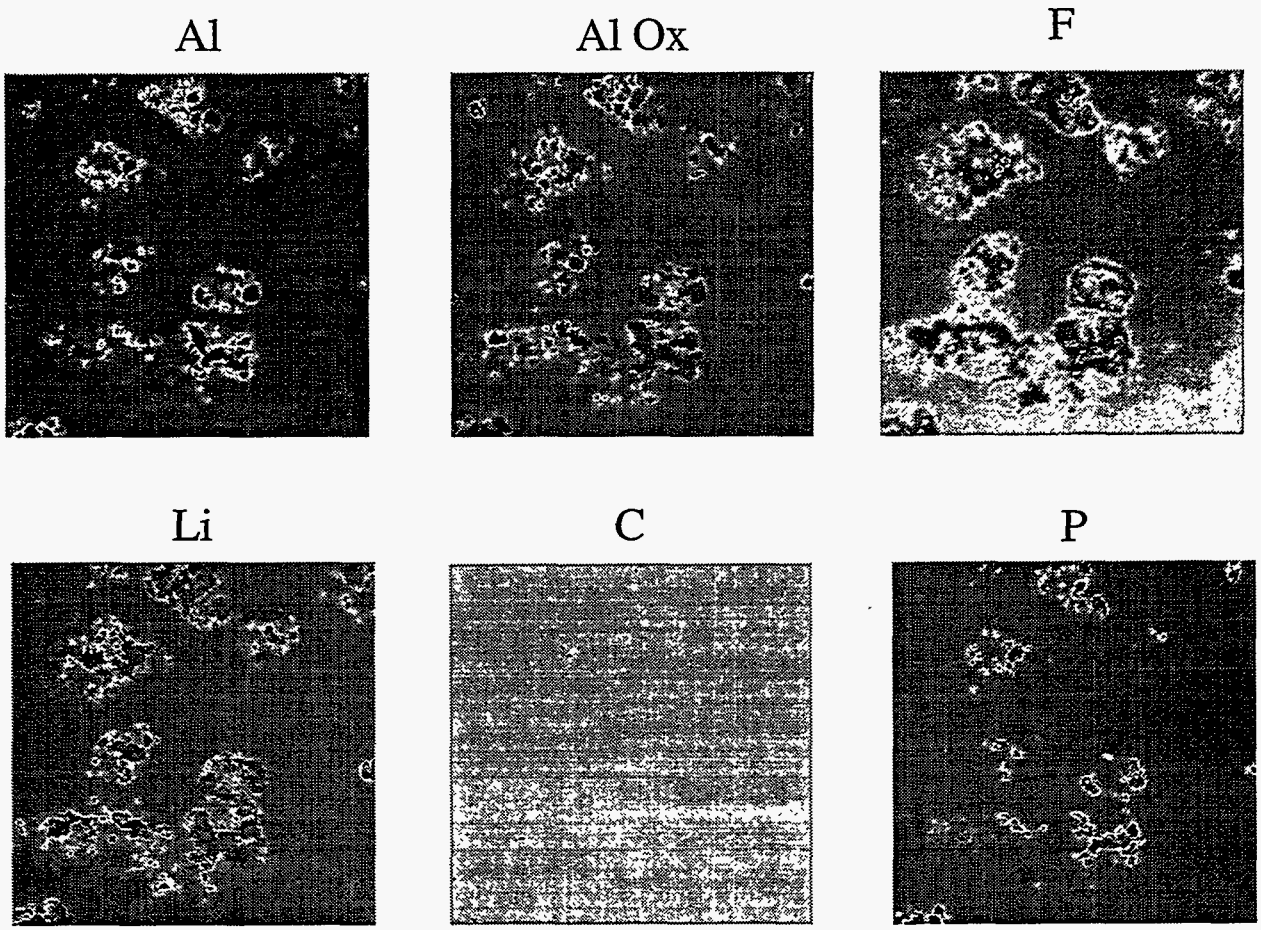

Figure 43. Auger maps of distributions of primary species identified on an Al 1100 electrode that had undergone 690 Leo cycles in PC:DEC electrolyte. The image size is 0.86 mm across edge.

Copper Environmental Cracking

To determine the susceptibility of copper to EAC, a series of constant extension rate tests was performed. The primary parameters that were studied included applied voltage, grain size, degree of work-hardening, and strain rate. An unsuccessful attempt was made to also include grain orientation.

Overall, only one combination of metallurgical and environmental conditions was identified that revealed a susceptibility of copper to intergranular EAC: work-hardening, a relatively large grain size, and an applied voltage of 0 volts vs. Li. Lack of any of these factors was sufficient to eliminate any interaction. The following figures illustrate the importance of the large grain size along with documenting the EAC susceptibility. The grain structure for two different copper

specimens is shown in Figures 44-47 and the respective SEM fracture surfaces are shown in Figures 48 and 49. Interestingly, intergranular cracking occurred in the large grained material despite an unfavorable orientation of the grains (longitudinally elongation). This occurrence is probably possible because of the severe CERT conditions. Relative to internal stress, the degree of work hardening was similar: large-grained susceptible sample: 116 VHN; small-grained sample: 119 VHN. The conditions under which a susceptibility is evident are consistent with those observed for Ni in $Li/SOCl_2$ cells [1], implying that the Cu EAC phenomenon is mechanistically similar, that is, Li-induced EAC.

No cracking of U-bend electrodes aged in flooded cells or actual foil from commercial cells has been observed (Figure 50 and 51). Thus, based on the results to date, the susceptibility to EAC can be eliminated by proper attention to metallurgical conditions.

CONCLUSIONS

The corrosion-related vulnerabilities of the primary current-collector materials being used in lithium-ion cells have been identified: aluminum - localized pitting; copper - environmentally assisted cracking. Localized pitting corrosion of aluminum positive-electrode current collectors occurs at the highly oxidizing potentials that exist around the top of charge. However, the pitting mechanism is more complex than that observed in aqueous systems probably due to the use of an organic electrolyte and the imposition of electrical cycling. For the first few hundred cycles, the PC:DEC electrolyte appears to be less corrosive than one composed with a EC:DMC solvent. Electrochemical impedance spectroscopy was shown to be an effective analytical tool to study corrosion behavior in these systems in that results correlate with visual observations and trends. Finally, two fluorocarbon-based coatings improved the short-term resistance of Al to localized pitting. Because these materials were aged for a maximum time of six months, the long-term effectiveness of these coatings was not established.

Detailed XPS and Auger analyses were performed to identify important species on the surface of the electrodes that could directly influence corrosion behavior. There was very little difference in the films observed after simple immersion in the electrolytes versus those resulting from electrically cycled half cells. Li is the predominant surface species. In general, about twice as much F is observed on the surface than would be present from the direct deposition of $LiPF_6$ from the electrolyte. Relative to electrolyte composition, the Al surfaces are very similar whether cycled in either PC:DEC or EC:DMC electrolytes. The primary difference observed is an increase in Cl (possibly B) in the EC:DMC formula electrolyte relative to the PC:DEC formula electrolyte. Based on these analyses, the role, if any, of surface species that are present due to exposure to the electrolyte was not determined. Possibly, the observed corrosion resistance of the aluminum is simply due to its native oxide layer. Changes in the thickness of the surface layer on aluminum were not determined. However, the surface layer on the copper was relatively thin (<150 Å) and did not thicken with cycling.

The copper negative current collector is susceptible to environmental cracking at or near the lithium potential only if specific metallurgical conditions exist (work hardening and large grain size). Although thin foils can possess conditions such as these, proper metallurgical control should eliminate any problems in practice.

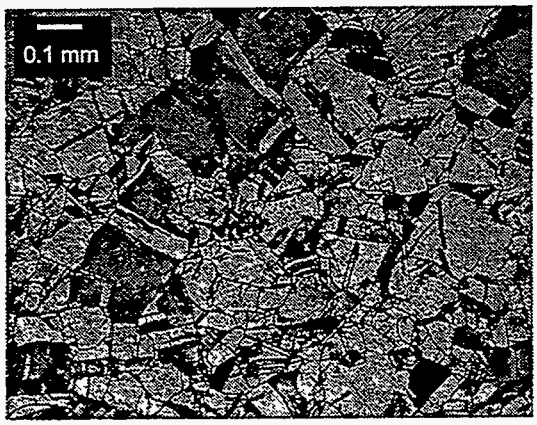

Figure 44. Optical photograph of transverse cross-sectioned copper tensile bar that did exhibit brittle behavior

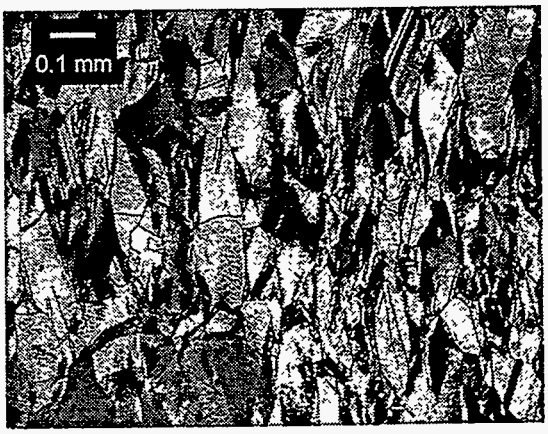

Figure 45. Optical photograph of longitudinal cross-sectioned copper tensile bar that did exhibit brittle behavior

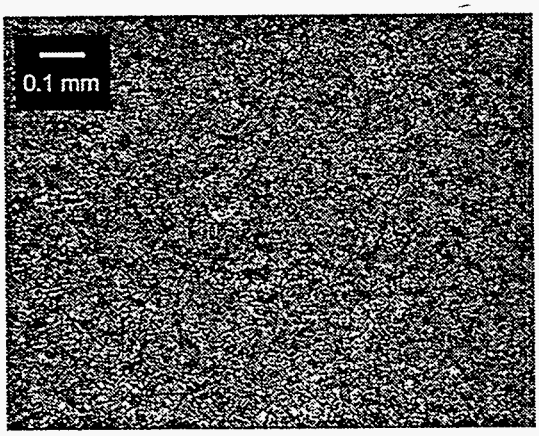

Figure 46. Optical photograph of transverse cross-sectioned copper tensile bar that did not exhibit brittle behavior

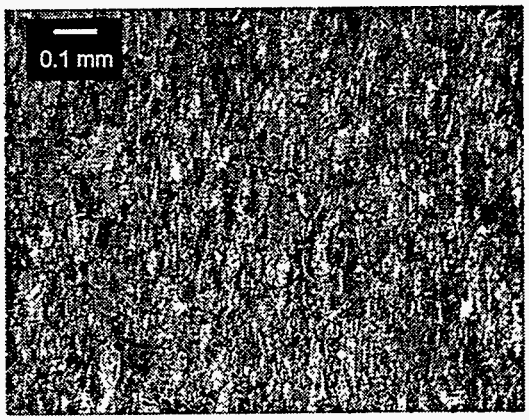

Figure 47. Optical photograph of longitudinal cross-sectioned copper tensile bar that did not exhibit brittle behavior

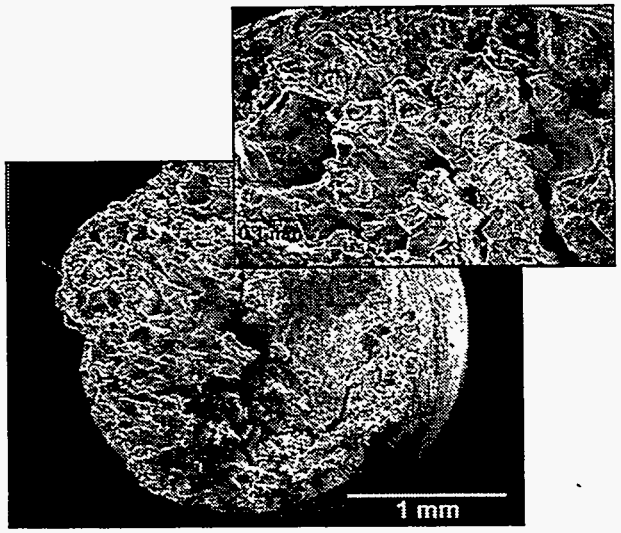

Figure 48. SEM photograph of the brittle fracture surface of coarse-grained, work-hardened copper

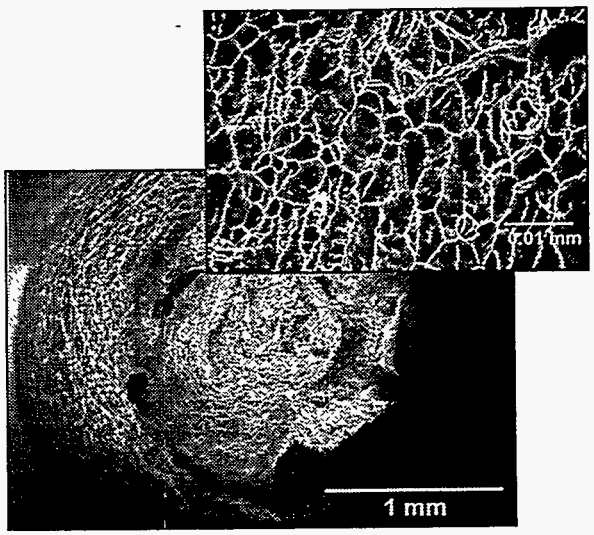

Figure 49. SEM photograph of the ductile fracture surface of fine-grained, work-hardened copper

Figure 50. Photograph of copper electrode that was plastically deformed and welded to help determine susceptibility to EAC (electrode width = 1 cm; LEO cycles = 100)

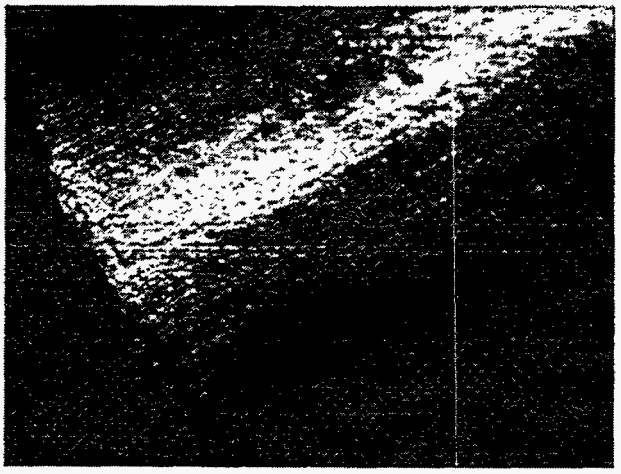

Figure 51. Closeup photograph of one edge of the copper U-bend electrode shown in Figure 50 (LEO cycles = 100)

FUTURE WORK

The objective of this initial phase of the study was to identify the major materials degradation issues. We believe that in general this work was successful. Nevertheless, we identified four areas for which additional attention would be warranted relative to this objective:

1. The length of time available for aging was not adequate to determine long-term effects. That is, the cells were aged for a maximum of 690 cycles and six months and none of the efforts to accelerate aging using temperature was successful. As such, the findings from this work apply primarily to the short-term.

2. A more sensitive EIS characterization technique for aluminum corrosion is needed. Given the high resistivity and stochastic corrosion nature of the aluminum, the work performed was at the limit of the instrumentation capabilities. To help with this situation, a larger working electrode, more replicated experiments, and a shortened time interval between EIS measurements are needed.

3. The matrix of conditions under which copper has a susceptibility to intergranular EAC was not quantified. Related is a design basis for conditions that would lead to actual cracking in cells. One potential solution would be to characterize the range of actual conditions that cause a susceptibility using u-bend samples of varying orientation and stress levels under various simulated cell environments

4. No optimization of the carbon coating process or surface pretreatment was performed.

Given that the principal vulnerability identified in this study was that the aluminum current collector undergoes pitting corrosion, the focus of any follow-on work must involve a determination of system-level effects of this corrosion on reliability and performance, if any. For example, the decreasing susceptibility to corrosion that was observed with continued cycling and could be due to a thickening film could have a negative effect in that an unacceptable increase in the long-term resistance of the cell could be produced. Alternately, the presence of mounds or nodules on the surface could lead to the delamination of active material. An associated, but critical activity, involves the identification of an effective accelerated aging technique. This effort is needed because, if corrosion is a problem, it does not emerge in the short-term. Finally, if a legitimate concern exists, solutions must be identified.

REFERENCES

1. R. Scully, et.al., *Journal of the Electrochemical Society*, 138, 2229, 1995.
2. R.K. Quinn and S. C. Levy, *24th National SAMPE Symposium Proceedings*, 229-237, May 1982.
3. A. Attewell, "Metallurgical Examination of Cracking in Buses from Lithium-Sulphur Dioxide Cells," *Royal Aircraft Establishment RAE(F)MT4/4/E1141*, May 1982.
4. R. G. Buchheit, et.al., "A Correlation Between Salt Spray and EIS Test Results for Conversion Coated Al Alloys," to be published in *Corrosion*, 1997 (in review)
5. A. Savitzky and M. J. E. Golay, *Anal. Chem.*, 36, 1627-1639, 1964
6. J. Steinier, Y. Termonia and J. Deltour, *Anal. Chem.*, 44, 1906-1909, 1972
7. H. H. Madden, *Anal. Chem.* 50, 1383-1386, 1978
8. C. D. Wagner, W. M. Riggs, L. E. Davis, J. F. Moulder and G. E. Muilenberg (Editor), *Handbook of X-ray Photoelectron Spectroscopy*, Perkin-Elmer Corporation, Eden Prairie, MN, 1979
9. W. B. Ebner and W. C. Merz, *Proceedings of the 29th Power Sources Symposium*, The Electrochemical Society, p. 265-280, 1980
10. D. A. Shifler, et.al., *Electrochimica Acta*, 40 (7), 897-905, 1995
11. J. F. Moulder, W. F. Stickle, P. E. Sobol, K. D. Bomben and J. Chastain (Editor), *Handbook of X-ray Photoelectron Spectroscopy*, 2nd edition, Perkin-Elmer Corporation, Eden Prairie, MN, 1992
12. C. D. Wagner and D. M. Bickham, "NIST X-ray Photoelectron Spectroscopy Database," *NIST Standard Reference Database 20*, National Institute of Standards and Technology, Gaithersburg, MD, 1989

ACKNOWLEDGMENTS

This work was supported by the United States Department of Energy under Contract DE-AC04-94AL85000. Sandia is a multiprogram laboratory operated by Sandia Corporation, a Lockheed Martin Company, for the United States Department of Energy. Specifically, grateful acknowledged for funding this Phase-I work is given to the DOE Office of Research and Development (NN-20) within the Office of Nonproliferation and National Security. The authors would like to also thank Rudy Buchheit and Rob Sorensen for their significant help with the experimental setup and the interpretation of corrosion data along with Dipesh Goel and Rudy Armijo for their assistance with the experiments and data reduction.

DISTRIBUTION

Danionics A/S
Attn: Rene Koksbang
Hestehaven 21 J
DK-5280 Odense S
Denmark

High Energy Technologies, Inc
Attn: Dr. Like Xie
2800 Hitchcock Ave.
Downers Grove, Il 60515

Hughes Research Labs
Attn: Anna M. Lackner
Dr. J. David Margerum
Batteries and Polymeric Sensors Department
Loc. MA; Bldg 254, M/S RL-70
3011 Malibu Canyon Road
Malibu, CA 90265-4799

Lockheed Martin Corp.
Attn: Mark Isaacson
Organization E6-01; Bldg 149
1111 Lockheed Way
Sunnyvale, CA 94089

Lockheed Martin Missiles and Space
Attn: Roger Hollandsworth
Organization H1-32; Bldg 204
3251 Hanover Street
Palo Alto, CA 94304

Lynntech, Inc.
Attn: Dr. Homayoun Moaddel
7610 Eastmark Driver, Suite 105
College Station, TX 77840

Rayovac Corporation
Attn: Edgar Armacanqui
David Fouchard
601 Rayovac Drive
Madison, WI 53711

U.S. Department of Energy
Attn: Gil Aeriola
Steven Herrick
Michael O'Connell
NN-20; Forrestal Bldg.
1000 Independence Ave.
Washington, DC 20585

U.S. Department of Energy
Attn: Dr. Albert R. Landgrebe
CE-142; 5E-036; Forrestal Bldg.
1000 Independence Ave.
Washington, DC 20585

University of California
Attn: Dr. James W. Evans
Department of Materials Science and Mineral Eng.
University of California at Berkeley
Berkeley, CA 94720

Yokohama R&D Laboratories
Attn: Hiro Tamura
Furukawa Electric Co.
2-4-3, Okano, Nshi-ku
Yokohama, 220 Japan

Sandia:

20	MS 0340	J. W. Braithwaite, 1832
1	MS 0340	W. R. Cieslak, 1832
1	MS 0340	S. J. Lucero, 1832
1	MS 0340	J. A. Ohlhausen, 1832
1	MS 0340	D. E. Peebles, 1832
1	MS 0571	R. L. Ewing, 5914
1	MS 0576	R. W. Moya, 5908
1	MS 0978	F. T. Noda, 5922
1	MS 0978	L. G. Stotts, 5934
1	MS 0978	J. P. Wolfe, 5921
1	MS 9403	W. R. Even, 8713
1	MS 9403	J. C. Wang, 8713
3	MS 0614	D. H. Doughty, 1521
3	MS 0614	G. Nagasubramanian, 1521
1	MS9018	Central Technical Files, 8940-2
5	MS0899	Technical Library, 4414
2	MS0619	Review and Approval Desk, 12690 for DOE/OSTI